Available online at www.sciencedirect.com
ScienceDirect
Trans. Nonferrous Met. Soc. China 24(2014) 2883−2889
Transactions of Nonferrous Metals Society of China
www.tnmsc.cn

Preparation of $ZrMn_2$ hydrogen storage alloy by electro-deoxidation in molten calcium chloride

Lei DAI[1,2], Shuo WANG[1], Ling WANG[1], Yao YU[1], Guang-jie SHAO[2]

1. College of Chemical Engineering, Hebei United University, Tangshan 063009, China;
2. State Key Laboratory of Metastable Materials Science and Technology, Yanshan University, Qinhuangdao 066004, China

Received 27 August 2013; accepted 27 November 2013

Abstract: $ZrMn_2$ alloy was electro-synthesized directly from cathode pellets compacted with powdered mixture of MnO_2 and ZrO_2 in molten calcium chloride. Sintering temperature, cell voltage and electrolysis time were the dominant factors that affected the characteristics of the final product. The results confirmed the formation of pure $ZrMn_2$ alloy through the electro-deoxidation of the mixed oxide pellets at 3.1 V for 12 h in 900 °C $CaCl_2$ melt. The X-ray diffraction (XRD) and cyclic voltammetry analysis suggested that the electro-deoxidation proceeded from the reduction of manganese oxides to Mn, followed by ZrO_2 or $CaZrO_3$ reduction on the pre-formed Mn to $ZrMn_2$ alloy. The cyclic voltammetry measurements using powder microelectrode showed that the prepared $ZrMn_2$ alloy has a good electrochemical hydrogen storage property.

Key words: electro-deoxidation; $ZrMn_2$ alloy; $CaCl_2$ melt; oxides; hydrogen storage property

1 Introduction

The Zr-based AB_2 type Laves phase alloys have been extensively investigated as promising hydrogen storage materials and metal hydride electrodes due to their fast kinetics, high storage capacity, easy activation and moderate working conditions [1−3]. A significant number of laboratory studies have been focused on their composition, structures, physicochemical properties and alloying effects [4−7]. Meanwhile, due to the continuous large scale use of the hydrogen storage alloys, some attentions have been paid to developing new preparation methods with low energy consumption and simple operation to cope with challenge from the soaring market prices of metals in recent years [8−10]. The dominant extractive metallurgy is focused on separately extracting and refining the individual metals, followed by melting, alloying and casting under vacuum. Such processes are high in energy consumption but low in production efficiency, contributing to the relatively high costs of the hydrogen storage materials.

The recent demonstration of direct electro-deoxidation of solid metal oxides in molten salts promises a novel generic technology, known as the FFC-Cambridge process, for the extraction of reactive metals in situ during electrolysis without going through any melting step [11−15]. Meanwhile, the other perceived advantages of the electro-deoxidation method include low energy consumption, simple operation, and the capability to directly reduce a combination of different metal oxides together to form alloys [16−19]. Some hydrogen storage alloys, such as $LaNi_5$ [20], $CeNi_5$ [21], $TbNi_5$ [22], $CeCo_5$ [23] and $ZrCr_2$ [24], have been successfully prepared by the electro-deoxidation method. Compared with hydrogen storage alloys prepared by other methods, the ones prepared by the FFC-Cambridge process exhibit comparable or better electro-hydrogen storage properties, and have easy preparation and low cost.

This work reported the success of applying the FFC-Cambridge process to preparation of $ZrMn_2$ alloy from their oxides. The influence of process parameters, such as sintering temperature, cell voltage and electrolysis time on the electrolysis process were investigated. The mechanism of the electro-deoxidation

Foundation item: Project (51201058) supported by the National Natural Science Foundation of China; Projects (E2010000941, E2014209009) supported by Hebei Provincial Natural Science Foundation of China
Corresponding author: Ling WANG; Tel/Fax: +86-315-2592170; E-mail: tswling@126.com
DOI: 10.1016/S1003-6326(14)63422-1

was proposed based on cyclic voltammetry curve using metallic cavity electrode in conjunction with X-ray diffraction (XRD) analysis.

2 Experimental

2.1 Preparation of cathode pellet

The oxide pellets were prepared by mixing commercial available powders of ZrO_2 and MnO_2 according to the stoichiometry of $ZrMn_2$. PVB (1%) and absolute alcohol were added to the mixture and thoroughly milled in a ball-milling container for 3 h. After drying, the mixture was pressed into pellets of 10 mm in diameter and 3 mm in thickness. And then the pellets were sintered at 900, 1050 and 1250 °C for 5 h, respectively. The composition and morphology of the sintered pellets were analyzed by XRD (Vantage 4.0) and SEM (S−4800), respectively.

2.2 Constant voltage electrolysis

The experimental apparatus used here was similar to that described in Ref. [21]. An alumina crucible was filled with about 800 g of a dehydrated $CaCl_2$ and placed at the bottom of a stainless steel reactor in a vertical furnace. Subsequently, argon gas was introduced into the reactor continuously. After the temperature increased to pre-set temperature, electrolysis of the oxide cathode with one or two pellets wrapped with Kanthal wire mesh proceeded at a constant voltage with high purity graphite used as the counter electrode. After electrolysis, the sample was lifted from the molten salt and cooled naturally in a stream of argon before removal from the steel reactor, and then was immediately washed in distilled water. The composition and morphology of the products were analyzed by XRD and SEM, respectively.

2.3 Cyclic voltammetry

Foil of molybdenum (width of 10 mm, thickness of 0.5 mm, length of 20 mm, purity of 99.9%) with one circular hole (diameter of 1.0 mm) was used for making the metallic cavity electrodes (MCE). The oxide powders manually filled into the MCE cavity by repeatedly finger-pressing were used as the working electrode on which cyclic voltammetry (CV) was then carried out in $CaCl_2$ melt at 900 °C. High purity graphite and Kanthal wire were used as the counter electrode and the pseudo-reference electrode, respectively. All electrochemical experiments were operated under the protection of an argon flow. The CVs were then recorded by ZAHNER IM6e electrochemical station.

2.4 Measurement of electrochemical hydrogen storage property

The electrochemical hydrogen storage property of $ZrMn_2$ alloy was investigated by CV experiments in a classical three-electrode cell. The powder microelectrode loading $ZrMn_2$ alloy was used as working electrode. A Pt plate and a Hg/HgO electrode were used as a counter electrode and a reference electrode, respectively.

3 Results and discussion

3.1 Influence of sintering temperatures

The cathode pellets sintered at different temperatures were analyzed using XRD. Figure 1 shows the variation of phases present in the precursor pellets after sintering at various temperatures. It was apparent that ZrO_2 kept stable and some change occurred to MnO_2 after sintering over the temperature range of 900−1250 °C. MnO_2 sintered at 900 °C was changed into Mn_2O_3 due to reaction (1). With the increase of sintering temperature, Mn_2O_3 was further reduced and Mn_3O_4 was formed at 1050 and 1250 °C, following reaction (2). Based on Gibbs free energy (ΔG^{Θ}) values for reactions (1) and (2) at the sintering temperatures, the two reactions could take place.

$$2MnO_2 = Mn_2O_3 + 1/2O_2,\quad \Delta G^{\Theta} = -40.646\ \text{kJ mol}^{-1},\ 900\ ^{\circ}\text{C} \tag{1}$$

$$3/2Mn_2O_3 = Mn_3O_4 + 1/4O_2,\quad \Delta G^{\Theta} = \begin{cases} -5.065\ \text{kJ/mol},\ 1050\,^{\circ}\text{C} \\ -13.436\ \text{kJ/mol},\ 1250\,^{\circ}\text{C} \end{cases} \tag{2}$$

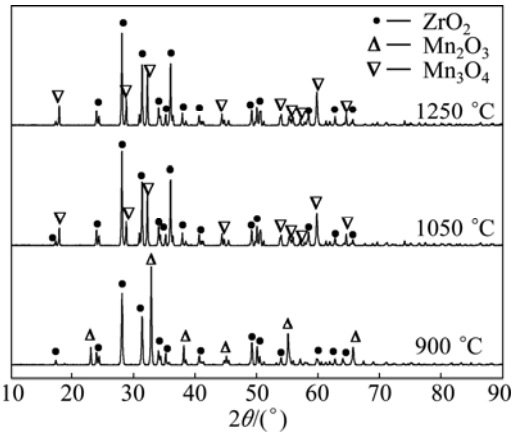

Fig. 1 XRD patterns of mixed oxide pellets sintered at various temperatures

Pellet sintering involves both increase of sample strength and shrinkage of volume, which can avoid powdering of the pellets in molten salt. Compared with the as-pressed ones, the sintered pellets became slightly smaller but much stronger. Figure 2 displays the SEM images of the mixed oxide pellets sintered at different temperatures. As shown in Fig. 2, the pellet porosity decreased with elevating sintering temperature and the particles grew up. The pellet had uniform small pores after being sintered at 900 °C. The pellet sintered at 1050

°C was more compact than the one sintered at 900 °C. At sintering temperature up to 1250 °C, it was clearly seen that a few of big pores appeared and particle size was quite big. The relatively large particle size meant a longer distance for oxygen ion transportation from particle inner to surface and hence a lower electro-deoxidation rate [21,25].

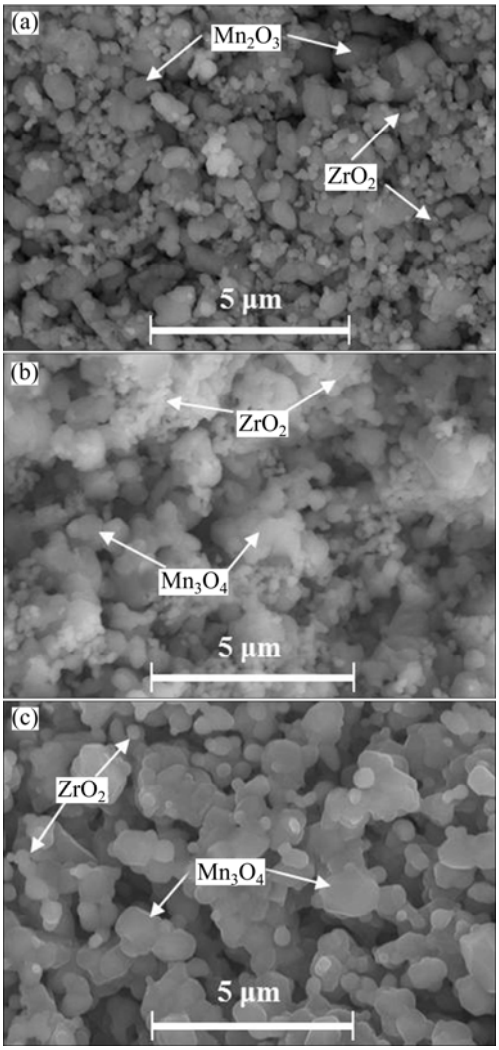

Fig. 2 SEM images of mixed oxide pellets sintered at 900 °C (a), 1050 °C (b) and 1250 °C (c) for 5 h, respectively

Figure 3 shows the typical current–time plots recorded during electrolysis of the oxide pellets sintered at different temperatures in 900 °C $CaCl_2$ melt. All current–time plots exhibited three steps. 1) In the first few minutes, electrolysis current increased along with time. When a constant cell voltage of 3.1 V was applied, the oxide in contact with the Kanthal wire began to reduce into metal, and then the new three-phase interlines (3PIs, metal/oxide/electrolyte) formed on pellet surface due to newly formed metal. With such processes continuing, the 3PIs expanded from the initial metal-oxide contact points along the pellet's surface, which increased the contact area of the metallic current collector and resulted in the increase of current [26]. 2) The current quickly declined in the 20−150 min. In this step, the 3PIs moving from surface into the interior of the oxide pellet and particles along the depth direction resulted in current decrease due to mass transfer difficulties [27]. 3) The current slowly declined to background value. In this step, the reduction reaction occurred in 3PIs of particles interior, so the electrolysis current slowly decreased down to background value. Due to electronic conduction through $CaCl_2$ melt, which resulted from the residue of the graphite particles and the impurity of the molten salt, the background current was zero [18,19]. The electrolysis current of the sample was dependent on sample sintering temperature. It was understood that the electro-deoxidization involved metal ion reduction and oxygen ion diffusion through the 3PIs. When the pellets were sintered at higher temperatures, the density and particle size increased, meaning the decrease of 3PIs length and oxygen ion transportation difficulty, and resulted in lower electro-deoxidation rate.

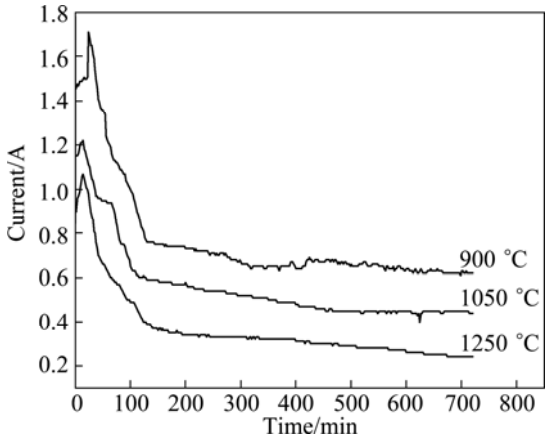

Fig. 3 Current–time plots of electrolysis of pellets sintered at different temperatures in 900 °C $CaCl_2$ melt at 3.1 V for12 h

Figure 4 shows the XRD patterns of the products from the mixed oxide pellets sintered at 900, 1050 and 1250 °C. It was clearly seen that after being electrolyzed at 3.1 V for 12 h, the pellet sintered at 900 °C was completely reduced to pure $ZrMn_2$ alloy. The reduced pellet could easily be ground into powder with pestle and mortar. As shown by the SEM image in Fig. 5, the product obtained after electrolysis for 12 h showed spongy and porous structure with the nodular particles, in agreement with previous findings in most metallized products from electro-reduction of solid metal oxides in $CaCl_2$ melt. As to the pellets sintered at 1050 and 1250 °C, XRD spectra showed that the electrolysis products were a mixture of $ZrMn_2$, Mn and $CaZrO_3$. The results further demonstrated that the sintering temperature increase does lead to lower reduction rate.

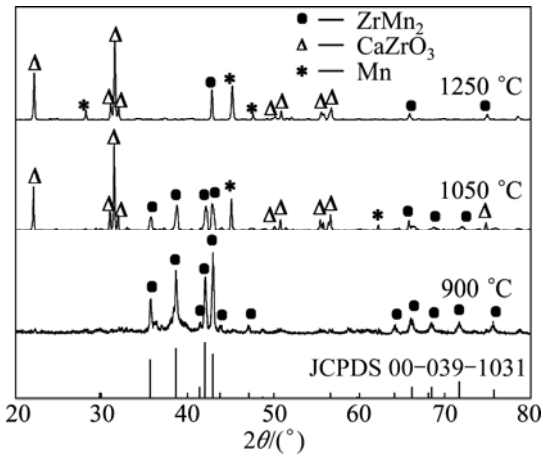

Fig. 4 XRD patterns of products from electrolysis of pellets sintered at different temperatures (3.1 V, 900 °C $CaCl_2$ melt, 12 h)

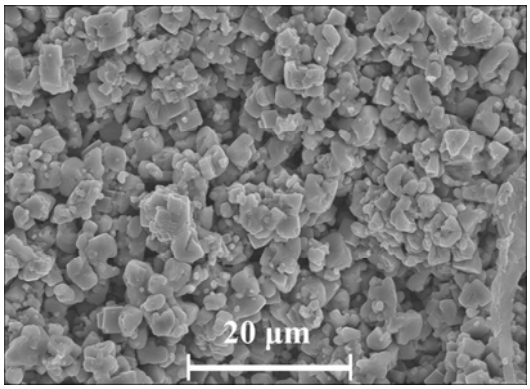

Fig. 5 SEM image of product from electrolysis of pellets sintered at 900 °C (3.1 V, 900 °C $CaCl_2$ melt, 12 h)

3.2 Influence of cell voltage

The principle for the choice of cell voltages is to avoid salt decomposition but achieve relatively high electro-deoxidation speed [22]. According to thermo-dynamic data, the decomposition voltages of ZrO_2, Mn_2O_3, Mn_3O_4 and $CaCl_2$ at 900 °C can be calculated.

$$Ca^{2+}+2e^{-}=Ca,\ \Delta E=3.23\ V \quad (3)$$

$$ZrO_2=Zr+O_2,\ \Delta E=2.37\ V \quad (4)$$

$$Mn_2O_3=2Mn+3/2O_2,\ \Delta E=1.13\ V \quad (5)$$

$$Mn_3O_4=3Mn+2O_2,\ \Delta E=1.27\ V \quad (6)$$

Based on above theoretical calculation, in this work, the cell voltages of 2.5, 2.8 and 3.1 V were chosen for the electro-deoxidation of the mixture oxide pellets. The XRD patterns of electrolysis products at different applied voltages are shown in Fig. 6. When 2.5 V was applied, the XRD spectrum of the product exhibited the Mn and $CaZrO_3$ phases, but no $ZrMn_2$ phase formed. At 2.8 V, the XRD spectrum of the product appeared to be $ZrMn_2$ phase. Meanwhile, there were still Mn, $CaZrO_3$ and traces of ZrO_2 phases, which meant that higher cell voltage was needed for the formation of pure $ZrMn_2$ phase. The XRD spectrum of the product after electrolysis at 3.1 V showed that pure $ZrMn_2$ phase was formed.

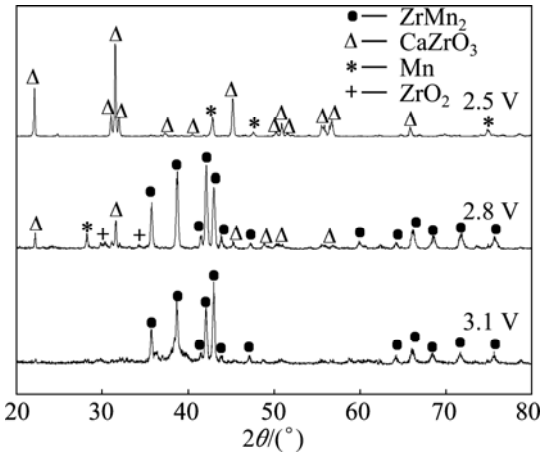

Fig. 6 XRD patterns of products from electrolysis of pellets sintered at 900 °C at different cell voltages for 12 h in 900 °C $CaCl_2$ melt

3.3 Analysis of electro-deoxidation process

To investigate the electrochemical reduction process of the mixed oxide pellets, the electrolysis of the pellets sintered at 900 °C was carried out at 3.1 V for different time and then the obtained products were analyzed by XRD.

Figure 7 shows the XRD patterns of the products that were electrolyzed at 3.1 V for 1, 4, 7, 10 and 12 h. In the first 1 h of electrolysis, the products were a mixture of ZrO_2, $CaZrO_3$, Mn_2O_3, Mn_3O_4 and Mn, but no $ZrMn_2$ was detected, which suggested that only Mn_2O_3 was reduced to Mn_3O_4 and Mn. After 4 h electrolysis, the $ZrMn_2$ phase began to appear. With a further increase in the electrolysis time, especially after 7 h, the $ZrMn_2$

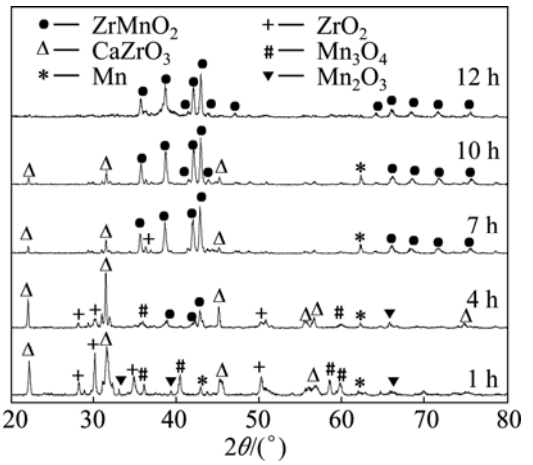

Fig. 7 XRD patterns of products from electrolysis of pellets sintered at 900 °C at 3.1 V for different time in 900 °C $CaCl_2$ melt

phase dominated in the product. After 12 h electrolysis, pure $ZrMn_2$ phase was detected. These results gave an indication of the formation of $ZrMn_2$ from the reduction of ZrO_2 or $CaZrO_3$ on the pre-formed Mn directly.

Based on the XRD results and previous studies on the mechanisms of the electro-reduction of solid metal oxides [21,28], the electro-deoxidation of ZrO_2−Mn_2O_3 to $ZrMn_2$ in $CaCl_2$ melt should have proceeded through the following steps.

$$3Mn_2O_3+2e=2Mn_3O_4+O^{2-} \quad (7)$$

$$Mn_3O_4+8e=3Mn+4O^{2-} \quad (8)$$

$$ZrO_2+Ca^{2+}+O^{2-}=CaZrO_3 \quad (9)$$

$$ZrO_2+2Mn+4e=ZrMn_2+2O^{2-} \quad (10)$$

$$CaZrO_3+2Mn+4e=ZrMn_2+Ca^{2+}+3O^{2-} \quad (11)$$

To further understand the electro-deoxidation process mechanism, the cyclic voltammograms of samples on the MCE were measured in $CaCl_2$ melt at 900 °C. Figure 8 shows the CVs of pure ZrO_2 powder, pure Mn_2O_3 powder and mixed ZrO_2 and Mn_2O_3 powders recorded in $CaCl_2$ melt at 900 °C. In the absence of oxide, the CV of the bare MCE showed a reduction peak c1 formed at −1.5 V until the potential scan was reversed which could be attributed to the reduction of $CaCl_2$ [22]. The voltammetric features of the pure ZrO_2 powders in the range from 0 to −0.65 V were similar to the ones of the bare MCE. Then the current became large, which suggested that the ZrO_2 or $CaZrO_3$ was reduced [29]. Compared with the bare MCE and ZrO_2 powders, the CV of the pure Mn_2O_3 powders exhibited larger current at potentials more negative than −0.1 V and a reduction peak c2 was formed at −0.8 V which could be attributed to the reduction of Mn_2O_3 into Mn metal. The voltammetric features of the mixed ZrO_2 and Mn_2O_3 powders were similar to those observed on the CV of the pure Mn_2O_3 powder in the range from 0 to −0.65 V and then the current became large and a peak, c3, was seen at −1.25 V which was absent on the CVs of the others. It was likely caused by the formation of the $ZrMn_2$ compound resulting from the reduction of ZrO_2 or $CaZrO_3$ on the newly formed Mn metal particles.

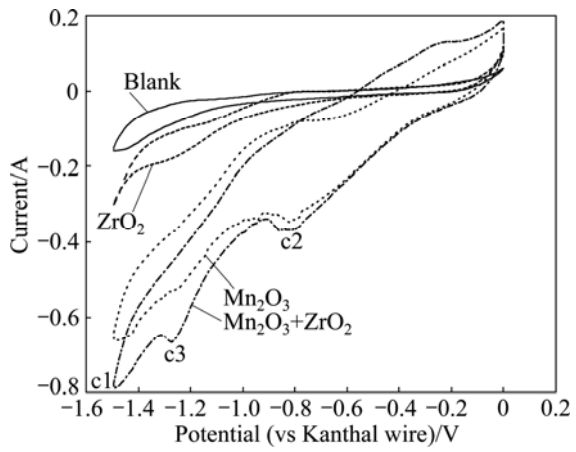

Fig. 8 Cyclic voltammograms of MCE without and with ZrO_2 powder, Mn_2O_3 powder and mixed ZrO_2 and Mn_2O_3 powders in 900 °C $CaCl_2$ melt (potential scanning rate: 10 mV/s)

3.4 Electrochemical hydrogen storage property

CV measurements were done at the potential ranging from −1200 to 0 mV (versus Hg/HgO electrode) to investigate the electrochemical hydrogen storage property of $ZrMn_2$ powders. Figure 9(a) illustrates the CV curves of the $ZrMn_2$ alloy powder microelectrode. The anodic peak (at −0.65 V) observed was due to the oxidation of the desorbed hydrogen atoms on the surface, which was used for evaluating the discharge processes of the $ZrMn_2$ alloy. The discharge capacities for sample can be calculated from the cyclic voltammograms based on previously reported method [30]. Figure 9(b) shows that discharge capacities depended on cycle number. The activation of $ZrMn_2$ was needed and almost completed after 20 cycles. The prepared $ZrMn_2$ had the best hydrogen storage property between 40 and 55 cycles. After 120 cycles the discharge capacity retention was approximately 96.7%.

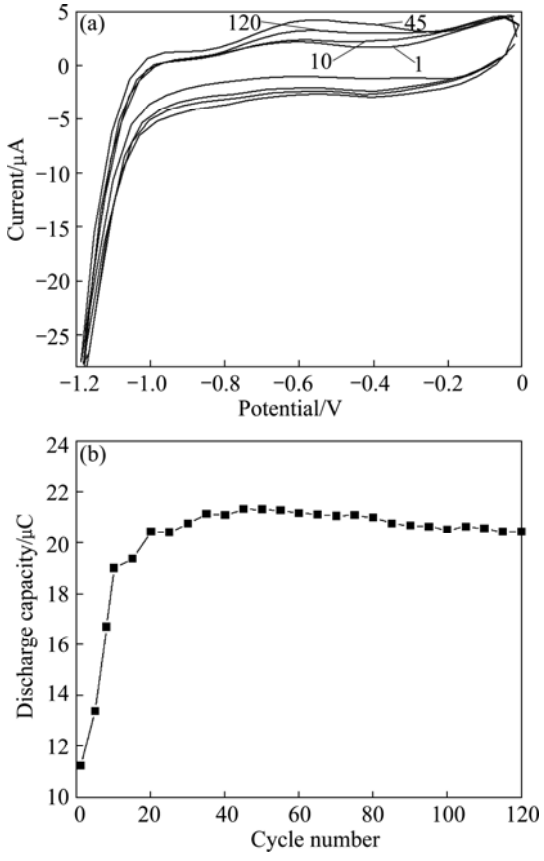

Fig. 9 Cyclic voltammograms of $ZrMn_2$ alloy powder microelectrode in 6 mol/L KOH solution (a) and discharge capacity versus cycle number (b) (potential scanning rate: 50 mV/s)

Compared with previously reported Zr-based hydrogen storage alloys [24,31,32], the electrolytic $ZrMn_2$ alloy exhibited comparable or better cycling stability, which might be attributed to the unique nodule-based porous structures with a large metal surface area for an enhanced interaction with H^+.

4 Conclusions

1) This work demonstrated a facile method for the fabrication of $ZrMn_2$ alloy powder from mixed oxides using the FFC-Cambridge process. Higher sintering temperature resulted in lower electro-deoxidation rate. The higher cell voltage favored the electro-deoxidation process. The pure $ZrMn_2$ alloy was obtained by electrolyzing a mixture of ZrO_2/MnO_2 in 900 °C $CaCl_2$ melt when 3.1V was applied for 12 h.

2) According to XRD and CVs analyses, the mechanism of the electro-deoxidation process could be divided into two steps: the reduction of mixed oxide started from manganese oxides to Mn, followed by ZrO_2 or $CaZrO_3$ reduction on the pre-formed Mn to form $ZrMn_2$ alloy.

3) The $ZrMn_2$ alloy powder for hydrogen storage showed good activity and cycling stability and the capacity retention was approximately 96.7% after 120 cycles.

References

[1] CUI X Y, LI Q, CHOU K C, CHEN S L, LIN G W, XU K D. A comparative study on the hydriding kinetics of Zr-based AB_2 hydrogen storage alloys [J]. Intermetallics, 2008, 16: 662−667.

[2] ANIKINA E Y, VERBETSKY V N. Investigation of $ZrMn_{2+x}$–H_2 by means of calorimetric method [J]. Journal of Alloys and Compounds, 2007, 446−447: 443−446.

[3] KIM J H, LEE H, HWANGA K T, HAN J S. Hydriding behavior in Zr-based AB_2 alloy by gas atomization process [J]. International Journal of Hydrogen Energy, 2009, 34: 9424−9430.

[4] HARA M, YUDOU K, KINOSHITA E, OKAZAKI K, ICHINOSE K, WATANABE K, MATSUYAMA M. Alloying effects on the hydride formation of $Zr(Mn_{1-x}Co_x)_2$ [J]. International Journal of Hydrogen Energy, 2011, 36: 2333−2337.

[5] KANDAVEL M, BHAT V V, ROUGIER A, AYMARD L, NAZRI G A, TARASCON J M. Improvement of hydrogen storage properties of the AB_2 Laves phase alloys for automotive application [J]. International Journal of Hydrogen Energy, 2008, 33: 3754−3761.

[6] PHILIPOSE S M, MANI N, KESAVAN T R, RAMAPRABHU S. Investigations of hydrogen storage properties in certain Zr-based AB_2 alloys [J]. International Journal of Hydrogen Energy, 2002, 27: 419−424.

[7] YOUNG K, OUCHI T, HUANG B, REICHMAN B, FETCENKO M A. The structure, hydrogen storage, and electrochemical properties of Fe-doped C14-predominating AB_2 metal hydride alloys [J]. International Journal of Hydrogen Energy, 2011, 36: 2296−2304.

[8] YOUNG K, KOCH J, OUCHI T, BANIK T A, FETCENKO M A. Study of AB_2 alloy electrodes for Ni/MH battery prepared by centrifugal casting and gas atomization [J]. Journal of Alloys and Compounds, 2010, 496: 669−677.

[9] CHU H L, ZHANG Y, SUN L X, QIU S J, XU F, YUAN H T. The electrochemical properties of $Ti_{0.9}Zr_{0.2}Mn_{1.5}Cr_{0.3}V_{0.3}$–$x$wt% $La_{0.7}Mg_{0.25}Zr_{0.05}Ni_{2.975}Co_{0.525}$ (x=0,5,10) hydrogen storage composite electrodes [J]. International Journal of Hydrogen Energy, 2007, 32: 1898−1904.

[10] MAKIHARA Y, UMEDA K, SHOJI F, KATO K, MIYAIRI Y. Cooperative dehydriding mechanism in a mechanically milled Mg−50mass% $ZrMn_2$ composite [J]. Journal of Alloys and Compounds, 2008, 455: 385−391.

[11] CHEN G Z, FRAY D J, FARTHING T W. Direct electrochemical reduction of titanium dioxide to titanium in molten calciumchloride [J]. Nature, 2000, 407: 361−364.

[12] JIANG K, HU X H, MA M, WANG D H, QIU G H, JIN X B, CHEN G Z. "Perovskitization"-assisted lectrochemical reduction of solid TiO_2 in molten $CaCl_2$ [J]. Angewandte Chemie International Edition, 2006, 45: 428−432.

[13] ABDELKADER A M, FRAY D J. Electro-deoxidation of hafnium dioxide and niobia-doped hafnium dioxide in molten calcium chloride [J]. Electrochimica Acta, 2012, 64: 10−16.

[14] SONG Q S, XU Q, KANG X, DU J H, XI Z P. Mechanistic insight of electrochemical reduction of Ta_2O_5 to tantalum in a eutectic $CaCl_2$−NaCl molten salt [J]. Journal of Alloys and Compounds, 2010, 490: 241−246.

[15] XIAO W, JIN X B, DENG Y, WANG D H, CHEN G Z. Rationalisation and optimisation of solid state electro-reduction of SiO_2 to Si in molten $CaCl_2$ in accordance with dynamic three-phase interlines based voltammetry [J]. Journal of Electroanalytical Chemistry, 2010, 639: 130−140.

[16] ZOU X L, LU X G, LI C H, ZHOU Z F. A direct electrochemical route from oxides to Ti−Si intermetallics [J]. Electrochimica Acta, 2010, 55: 5173−5179.

[17] ZHANG Qing-jun, QU Mei-ling, WANG Ling, DAI Lei, TIAN Ying, CUI Chun-xiang. Preparation of CoSn alloy by electro- deoxidization in molten salt [J]. The Chinese Journal of Nonferrous Metals, 2010, 20(8): 1578−1582. (in Chinese)

[18] ABDELKADER A M, FRAY D J. Direct electrochemical preparation of Nb−10Hf−1Ti alloy [J]. Electrochimica Acta, 2010, 55: 2924−2931.

[19] PANIGRAHI M, SHIBATA E, IIZUKA A, NAKAMURA T. Production of Fe−Ti alloy from mixed ilmenite and titanium dioxide by directelectrochemical reduction in molten calcium chloride [J]. Electrochimica Acta, 2013, 93: 143−151.

[20] ZHU Y, WANG D H, MA M, HU X H, JIN X B, CHEN G Z. More affordable electrolytic $LaNi_5$-type hydrogen storage powders [J]. Electrochemistry Communications, 2007, 24: 2515−2517.

[21] ZHAO B J, WANG L, DAI L, CUI G H, ZHOU H Z, KUMAR R V. Direct electrolytic preparation of cerium/nickel hydrogen storage alloy powder in molten salt [J]. Journal of Alloy and Compounds, 2009, 468: 379−385.

[22] QIU G H, WANG D H, JIN X B, CHEN G Z. A direct electrochemical route from oxide precursors to the terbium–nickel intermetallic compound $TbNi_5$ [J]. Electrochimica Acta, 2006, 51: 5785−5793.

[23] DAI Lei, WANG Shuo, LI Yue-hua, WANG Ling, SHAO Guang-jie. Direct electrochemical preparation of $CeCo_5$ alloy from mixed oxides [J]. Transactions of Nonferrous Metals Society of China, 2012, 22: 2007−2013

[24] PENG J J, ZHU Y, WANG D H, JIN X B, CHEN G Z. Direct and low energy electrolytic co-reduction of mixed oxides to zirconium-based multi-phase hydrogen storage alloys in molten salts [J]. Journal of Materials Chemistry, 2009, 19: 2803−2809.

[25] GORDO E, CHEN G Z, FRAY D J. Toward optimisation of electrolytic reduction of solid chromiumoxide to chromium powder in molten chloride salts [J]. Electrochimica Acta, 2004, 49:

2195−2208.

[26] DENG Y, WANG D H, XIAO W, JIN X B, HU X H, CHEN G Z. Electrochemistry at conductor/insulator/electrolyte three-phase interlines: A thin layer model [J]. Journal of Physical Chemistry B, 2005, 109: 14043−14051.

[27] YIN H Y, YU T, TANG D Y, RUAN X F, ZHU H, WANG D H. Electrochemical preparation of NiAl intermetallic compound from solid oxides in molten $CaCl_2$ and its corrosion behaviors in NaCl aqueous solution [J]. Materials Chemistry and Physics, 2012, 133: 465−470.

[28] PENG J J, CHEN H L, JIN X B, WANG T, WANG D H, CHEN G Z. Phase-tunable fabrication of consolidated (α+β)-TiZr alloys for biomedical applications through molten salt electrolysis of solid oxides [J]. Chemistry of Materials, 2009, 21: 5187−5195.

[29] PENG J J, LI G M, CHEN H L, WANG D H, JIN X B, CHEN G Z. Cyclic voltammetry of ZrO_2 powder in the metallic cavity electrode in molten $CaCl_2$ [J]. Journal of the Electrochemical Society, 2010, 157: F1−F9.

[30] HAN Jing, YANG Yi-fu, TAN Zu-xian, SHAO Hui-xia. Structure and activation performance of $La_{1-x}Ce_xNi_5$ hydrogen storage alloy [J]. The Chinese Journal of Nonferrous Metals, 2006, 16(11): 1861−1868. (in Chinese)

[31] TRIACA W E, PERETTI H A, CORSO H L, BONESI A , VISINTIN A. Hydrogen absorption studies of an over-stoichiometric zirconium-based AB_2 alloy [J]. Journal of Power Sources, 2003, 113: 151−156.

[32] ZHANG Yang-huan, LI Ping, WANG Xin-lin, QI Yan, LIN Yu-fang, WANG Guo-qing. The effect of rapid quenching on the cycle lives of H_2-storage electrode alloys with AB_2 laves phase [J]. Rare Metal Materials and Engineering, 2004, 33(12): 1321−1324. (in Chinese)

熔盐电脱氧法制备 $ZrMn_2$ 储氢合金

戴 磊[1,2]，王 硕[1]，王 岭[1]，余 瑶[1]，邵光杰[2]

1. 河北联合大学 化学工程学院，唐山 063009；
2. 燕山大学 亚稳材料制备技术与科学国家重点实验室，秦皇岛 066004

摘 要：采用熔盐电脱氧法，由 MnO_2 和 ZrO_2 混合氧化物直接合成 $ZrMn_2$ 合金。研究烧结温度、电解电压及电解时间等工艺参数对产物组成的影响。在 900 °C 的 $CaCl_2$ 熔盐中，经 900 °C 烧结的混合氧化物阴极在 3.1 V 恒电压下电解 12 h，可制备出纯相的 $ZrMn_2$ 合金。XRD 和循环伏安结果表明，在电解过程中，Mn−O 化合物首先还原成单质 Mn, ZrO_2 和 $CaZrO_3$ 再在单质 Mn 表面还原，并与其合金化，形成 $ZrMn_2$ 合金。以粉末微电极为工作电极，循环伏安测试结果表明，所制备的 $ZrMn_2$ 合金表现出良好的电化学储氢性能。

关键词：电脱氧；$ZrMn_2$ 合金；$CaCl_2$ 熔盐；氧化物；储氢性能

(Edited by Hua YANG)